Icarus 211 (2011) 259–272

Contents lists available at ScienceDirect

Icarus

journal homepage: www.elsevier.com/locate/icarus

A geomorphic analysis of Hale crater, Mars: The effects of impact into ice-rich crust

A.P. Jones [a,*], A.S. McEwen [b], L.L. Tornabene [b,1], V.R. Baker [c], H.J. Melosh [d], D.C. Berman [e]

[a] Department of Geosciences, University of Arizona, Tucson, AZ 85721, United States
[b] Lunar and Planetary Laboratory, University of Arizona, Tucson, AZ 85721, United States
[c] Department of Hydrology and Water Resources, University of Arizona, Tucson, AZ 85721, United States
[d] Department of Earth and Atmospheric Sciences, Purdue University, West Lafayette, IN 47907, United States
[e] Planetary Science Institute, 1700 East Fort Lowell Road, Suite 106, Tucson, AZ 85719, United States

ARTICLE INFO

Article history:
Received 23 April 2010
Revised 13 October 2010
Accepted 15 October 2010
Available online 29 October 2010

Keywords:
Mars
Mars, Surface
Impact processes

ABSTRACT

Hale crater, a 125 × 150 km impact crater located near the intersection of Uzboi Vallis and the northern rim of Argyre basin at 35.7°S, 323.6°E, is surrounded by channels that radiate from, incise, and transport material within Hale's ejecta. The spatial and temporal relationship between the channels and Hale's ejecta strongly suggests the impact event created or modified the channels and emplaced fluidized debris flow lobes over an extensive area (>200,000 km^2). We estimate ~10^{10} m^3 of liquid water was required to form some of Hale's smaller channels, a volume we propose was supplied by subsurface ice melted and mobilized by the Hale-forming impact. If 10% of the subsurface volume was ice, based on a conservative porosity estimate for the upper martian crust, 10^{12} m^3 of liquid water could have been present in the ejecta. We determine a crater-retention age of 1 Ga inside the primary cavity, providing a minimum age for Hale and a time at which we propose the subsurface was volatile-rich. Hale crater demonstrates the important role impacts may play in supplying liquid water to the martian surface: they are capable of producing fluvially-modified terrains that may be analogous to some landforms of Noachian Mars.

1. Introduction

Hale crater, a 125 × 150 km impact crater located at 35.7°S, 323.6°E on the northern rim of Argyre basin (Fig. 1), is surrounded by channels that radiate from, incise, and transport material within Hale's ejecta. Hale is one of the largest martian craters presently known to have impact-related channels. The channels' spatial and temporal connection with the crater strongly suggests they were created or heavily modified by the Hale-forming impact. The amount of water-rich debris required to carve or modify the channels requires a volatile-rich layer at the impact site that we propose was primarily subsurface ice.

Several authors have linked the formation of channels with impact events (e.g. Maxwell et al., 1973; Brakenridge et al., 1985; McEwen et al., 2007b; Tornabene et al., 2007b; Williams and Malin, 2008; Morgan and Head, 2009), yet the number of craters with impact-generated fluvially-modified forms, such as Mojave (7.6°N, 327.0°E), Tooting (23.4°N, 207.5°E), Zunil (7.7°N, 166°E), and Sinton (40.4°N, 31.4°E) (Williams et al., 2006; Williams and Malin, 2008; McEwen et al., 2007b; Tornabene et al., 2007a; Morgan and Head, 2009), remains small. These craters are all very well preserved, as is Hale crater: Hale's fresh appearance in nighttime infrared (IR) and visible images, as well as the relatively few superimposed craters, indicate that it may be one of the youngest craters of its size on Mars (Tornabene et al., 2008a,b). Channels associated with older, more degraded craters may have been modified beyond recognition.

In the following sections we (1) present a morphologic map of Hale, emphasizing the channels emanating from its ejecta blanket; (2) estimate peak flow velocities and discharges in some of Hale's channels to constrain the amount of water released; (3) consider possible sources for the water; and (4) determine the crater-retention age within Hale's primary cavity, thus estimating a minimum age for the Hale impact event.

2. Geologic setting

Hale is a complex crater with a central peak and multiple wall terraces (Melosh, 1989). The rim and terrace structures are clearly defined in the northern part of the crater. Hale was likely formed by an oblique impact from the southeast, due to its elongated northwest–southeast shape, its asymmetric ejecta blanket (Herrick and Hessen, 2006), its asymmetric central peak complex (peak size and elevation increases from southeast to northwest), and the distribution of secondary craters and streaks. The topographic slope of Argyre basin also influenced Hale's morphology.

* Corresponding author. Present address: Lunar and Planetary Institute, Houston, TX 77058, United States.
E-mail address: ajones@lpi.usra.edu (A.P. Jones).
[1] Present address: Center for Earth and Planetary Studies, Smithsonian Institution, Washington, DC 20013, United States.

0019-1035/$ - see front matter © 2010 Elsevier Inc. All rights reserved.
doi:10.1016/j.icarus.2010.10.014

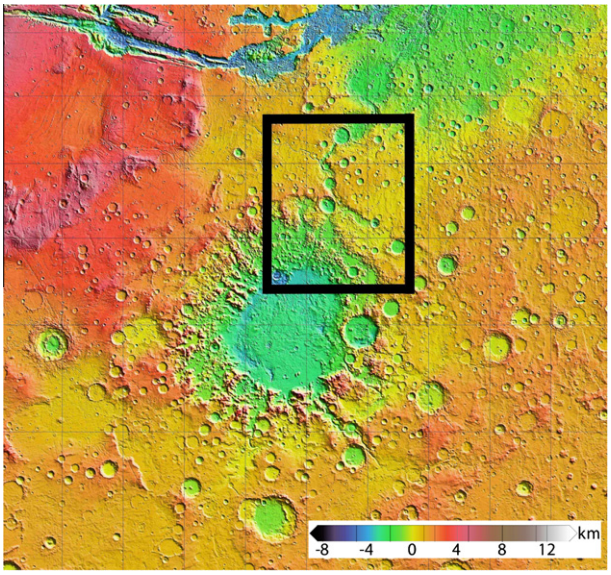

Fig. 1. *Location of mapping area.* The geomorphic map of Hale crater is a 20° × 20° region centered on Hale (35.7°S, 323.6°E), pictured here within a 100° × 65° MOLA elevation map (5–70°S, 270–10°E) shown in a Mercator projection. North is to the top in this and all subsequent images, unless otherwise indicated. Argyre basin opens to the southwest from Hale's location, and Vallis Marineris is to the northwest. Image credit MOLA homepage: http://www.mola.gsfc.nasa.gov.

The landscape surrounding Hale has been sculpted by water. The Hale-forming bolide impacted the northern rim of Argyre basin at its intersection with what may be an extension of Uzboi Vallis, part of the Uzboi-Ladon-Morava (ULM) outflow system (Figs. 1 and 2); see Section 3.5 for discussion. The ULM is thought to have periodically transported large volumes of water (~150,000–450,000 $m^3 s^{-1}$) during late Noachian through early Hesperian time (Grant and Parker, 2002). A large lake once occupied Uzboi Vallis between Bond and Holden craters. This lake overflowed and flooded Holden crater (Grant and Parker, 2002; Grant et al., 2010). Nirgal Vallis, interpreted as a groundwater sapping channel (Baker, 1980; Jaumann and Reiss, 2002), is ~700 km long and ~300 km from Hale. Smaller channels of various sizes, morphologies, and degradation states are also found in the area. Clearly, water was once abundant in this region. Gullies within Hale and nearby craters suggest recent activity, and may indicate the continued presence of water (e.g. Malin and Edgett, 2000; McEwen et al., 2007b; Kolb et al., 2010).

Surrounding Hale, relatively smooth (at 100 m $pixel^{-1}$) cratered plains extend beyond the rim of Argyre to the north, and chaotic, hummocky terrain characterizes the slope of the ancient basin to the south.

3. Geomorphic map of Hale crater

To study the relationship of Hale crater and its channels, we first constructed a geomorphic map of Hale crater (Fig. 2) using data and imagery from the Mars Orbital Camera (MOC, Malin and Edgett, 2001), the Mars Orbiter Laser Altimeter (MOLA, Smith et al., 2001), daytime and nighttime IR imagery from the Thermal Emission Imaging System (THEMIS, Christensen et al., 2004), the Context Camera (CTX, Malin et al., 2007), and the High Resolution Imaging Science Experiment (HiRISE, McEwen et al., 2007a). The base map is a ~100 m $pixel^{-1}$ THEMIS daytime-IR mosaic (Christensen et al., 2004) with a sinusoidal projection centered on Hale's latitude. Units relating to Hale crater are mapped at 1:500,000 based on geomorphology and thermophysical properties. The map provides an overview of Hale crater and context for analyzing Hale's channels.

Channels associated with Hale, two types of ejecta, ponded and pitted material, exposed rock, and irregular crater clusters (interpreted to be Hale's secondary craters) have been mapped (Fig. 3) and are described below. Pre-existing chaotic terrain on the margin of Argyre basin, post-impact mantling materials, and periglacial modification make unit boundaries less clear to the south of Hale than to its north.

3.1. Hale ejecta types 1 and 2

Hale ejecta types 1 (He1) and 2 (He2) dominate the geomorphic map of Hale crater. He1 is the proximal ejecta unit and is rough at map scale. He2 is smoother, thinner, and farther from the primary crater than He1. Both ejecta units flowed across and modified the surface. An example of this is where ejecta breached the eastern rim of a pre-existing crater just west of Hale, filled the crater, and then flowed out the other side (Fig. 5). Viscous flow features within both ejecta units are found all around the crater, roughly radial to the primary cavity and roughly parallel to lineations within the ejecta blanket, though they are strongly influenced by local topography. Most of Hale's channels originate at the distal edges of He1 or within He2.

He1 is interpreted to be a combination of ballistic and ground-hugging ejecta. The ground-hugging component of He1 flowed downhill and around positive-relief features. Long chains of elongated craters that radiate from Hale and scoured the surrounding surface are found within He1. These crater chains are particularly abundant northeast of Hale crater (Fig. 6); the long axes of the craters are oriented towards Hale. Additional pitting in distal He1 may result from warm ejecta interacting with frozen, possibly snow- or ice-covered ground, or post-emplacement melting or sublimation of blocks of ice in the ejecta (Mouginis-Mark, 1987). He1 surrounds Hale's main crater cavity, and also collected inside it. Pits in He1 ejecta that ponded within Hale crater and behind its rim terraces may be collapse pits formed from volatile release; see Section 3.2 for discussion. A fine-scale pitting pervades He1 at HiRISE resolution. The craters and pits within this ejecta unit make this unit appear rough in visible imagery, and the pattern is observable in thermal inertia data as well (Fig. 6).

He2 appears to be a thinner, more mobile, distal ejecta unit that emanates from He1 (Fig. 6). He2 is smooth at map scale and generally appears smooth even at HiRISE resolution, though a small-scale pitted texture is sometimes found where it has collected in low-lying areas. Pre-existing terrain beneath He2 is less obscured than that beneath He1. He2 is most abundant on the sloping topography of Argyre basin, southwest of Hale (Figs. 2 and 11). The observations that He2 is smooth at map scale and grades into the surrounding terrain at the highest-resolution imagery available are consistent with the interpretation of He2 as a thinner, more mobile (lower viscosity or yield strength), and more volatile-rich ejecta unit than He1.

Although Hale possesses two distinct ejecta units, Hale is not a typical double-layered ejecta (DLE) crater (Barlow et al., 2000). Hale's 138-km average diameter is much larger than the maximum DLE crater diameters in studies by Barlow and Bradley (1990) and Boyce and Mouginis-Mark (2006) (50 km and 29.6 km, respectively). Hale has an abundance of nearby overlapping chains of secondary craters, which DLE craters seem to lack. A rough radial texture visible in Hale's inner ejecta differs from the clean lines that define the radial texture in both ejecta units of DLE craters (Barlow et al., 2000; Boyce and Mouginis-Mark, 2006). Additionally, Boyce and Mouginis-Mark (2006) proposed that the outer ejecta unit of DLE craters is composed of fine-grained, loosely consolidated materials emplaced by impact-generated high winds, while Hale's outer ejecta unit appears to have flowed over the surface at lower velocities.

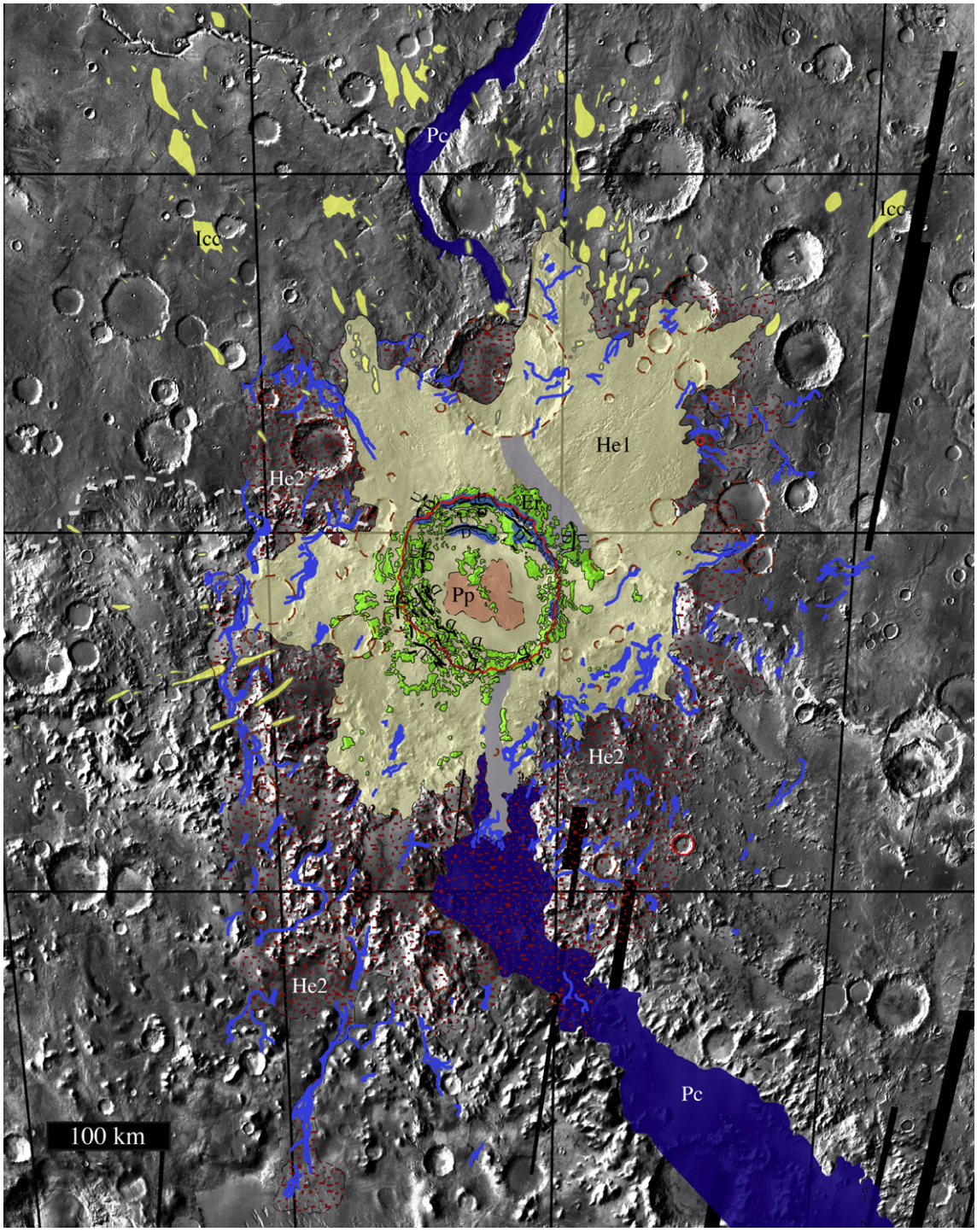

Fig. 2. *A geomorphic map of Hale crater*. Units related to Hale (listed in Fig. 3) are mapped on a 1:500,000 THEMIS daytime-IR mosaic with a resolution of ~100 m pixel^{-1} in a sinusoidal projection centered on Hale's latitude. (THEMIS mosaics, used here and in Figs. 4–6, 8, 12 and 18 are available at http://www.global-data.mars.asu.edu/bin/themis.pl.) Rims of craters >5 km in diameter found within He1 and He2 are also mapped: rims of craters that overprint Hale ejecta are marked as fresh craters; craters discernable beneath Hale's ejecta are mapped as buried crater rims. The Hale-crater-forming bolide impacted the intersection of Uzboi Vallis (Pc north of Hale crater), a potential extension of Uzboi Vallis (Pc that continues south of Hale crater), and the northern rim of Argyre basin (mapped as the dominant regional slope break). The blue lines trace channels carved or heavily modified by water mobilized in the Hale-forming impact event. A subset of the full 20° × 20° map area is shown here. (For interpretation of the references to color in this figure legend, the reader is referred to the web version of this article.)

3.2. Ponded and pitted material

Coalescing groups of subcircular pits that lack both raised rims and ejecta are found in ponded materials within and around Hale crater. This *ponded and pitted material* is most abundant on the floor of Hale, but is also observed in topographic depressions outside the crater rim and behind rim terraces. The material with the largest pits (tens to hundreds of meters in diameter) is distinguished as a separate unit (*Pp*) from the other pitted materials within He1 (Fig. 7), and may mark thicker deposits (Bray et al., 2009). Though not visible at map scale, fractures cross this unit that may have been produced by material cooling and contracting (Mouginis-Mark and Garbeil, 2007; Mouginis-Mark et al., 2007; Tornabene et al., 2007a).

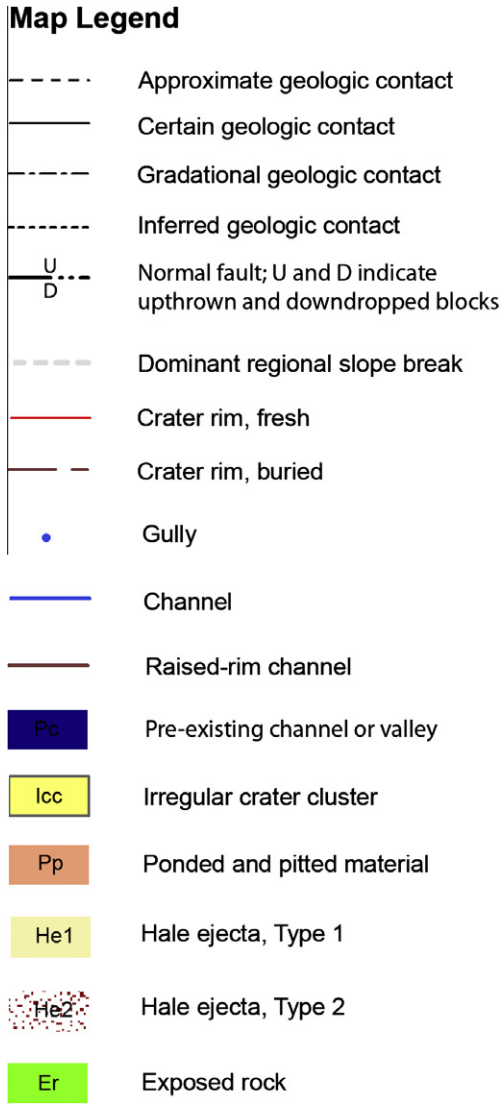

Fig. 3. *Map legend*. Units and symbols in the geomorphic map of Hale crater (Fig. 2). See text for unit descriptions.

Similar pits within well-preserved impact craters described by McEwen et al. (2007b), Mouginis-Mark et al. (2007), Tornabene et al. (2007b), and Bray et al. (2009) are interpreted as collapse pits formed by volatiles escaping from a mixture of impact melt and lithic clasts. These materials lithify to form impact melt breccias also known as suevite (e.g. McEwen et al., 2007b; Tornabene et al., 2007b; Bray et al., 2009). The concentration of Pp at the lowest elevations of Hale crater, where a thick deposit of hot ejecta materials would have accumulated, supports this hypothesis (Fig. 11).

3.3. Exposed rock

He1 overlies a rugged, blocky, resistant unit of *exposed rock (Er)*. This unit is found at the highest elevation areas in Hale crater, including its rim, wall terraces, and central peak complex. This cliff-forming unit is overlain by colluvium, and gullies originate on its steep slopes. Er appears smoother and more rounded further from Hale crater. Its blocky appearance within the crater may result from high shock pressures that fractured rock at and near the impact site during crater formation. We interpret this unit as bedrock that predates the formation of Hale crater, and loose rocks that originated from nearby bedrock.

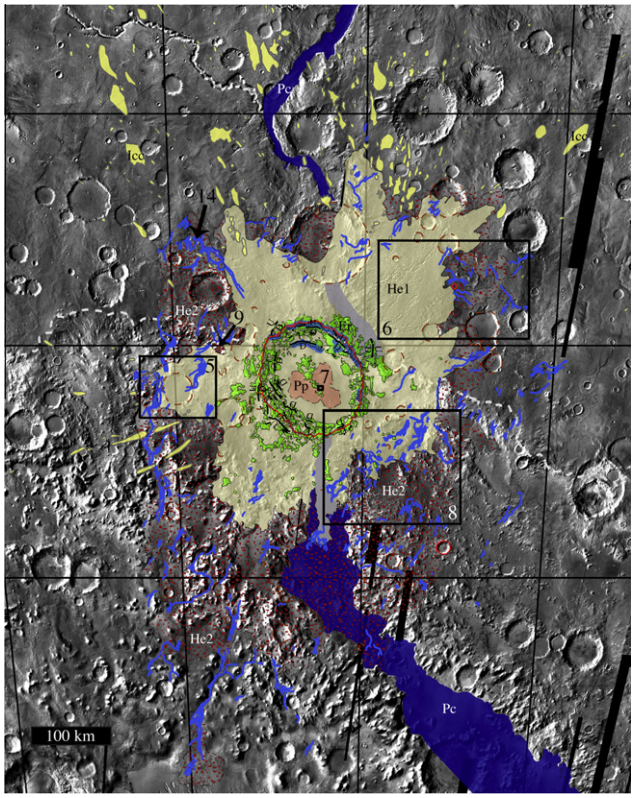

Fig. 4. *Figure location map*. Geomorphic map of Hale overlain with boxes and arrows indicating the locations of subsequent images. Numbers correspond with figure numbers.

3.4. Irregular crater clusters

Dense clusters of irregular craters all exhibiting similar, fairly low levels of degradation are mapped as *irregular crater clusters (Icc)*. These clusters are organized into overlapping chains of craters with herringbone patterns in their ejecta (e.g. Shoemaker, 1962; Oberbeck and Morrison, 1973) that radiate from Hale and point back to this crater. Long axes of individual craters within the clusters are also oriented toward Hale's primary cavity. These crater clusters are interpreted to be Hale secondary craters. They are found primarily northwest to northeast of Hale and extend beyond the map area.

Most secondaries that lie within He1 and He2 appear to be filled with ejecta, indicating ballistic ejecta emplacement was followed by surface flow, in agreement with Herrick and Hessen (2006). The rough terrain within He1 northeast of Hale makes it difficult to determine whether this depositional sequence holds in this area. If this rough texture is attributed to overprinting by ballistic ejecta, it would support the multi-layered hypothesis of Barlow and Bradley (1990), where lobate ejecta containing near-surface volatiles is emplaced first, with ballistic ejecta following once the impactor excavated deeper, and perhaps drier material beneath an icy layer.

3.5. Channels

Channels within or emanating from Hale's ejecta are generally immature, exhibiting primitive branching patterns. Many channels have a braided morphology, and some contain streamlined "islands" (that may have been submerged during peak flow). The channels transported ejecta materials from Hale crater: impact ejecta flowed into and through the channels. The channels are topographically controlled, flowing downhill and around obstacles,

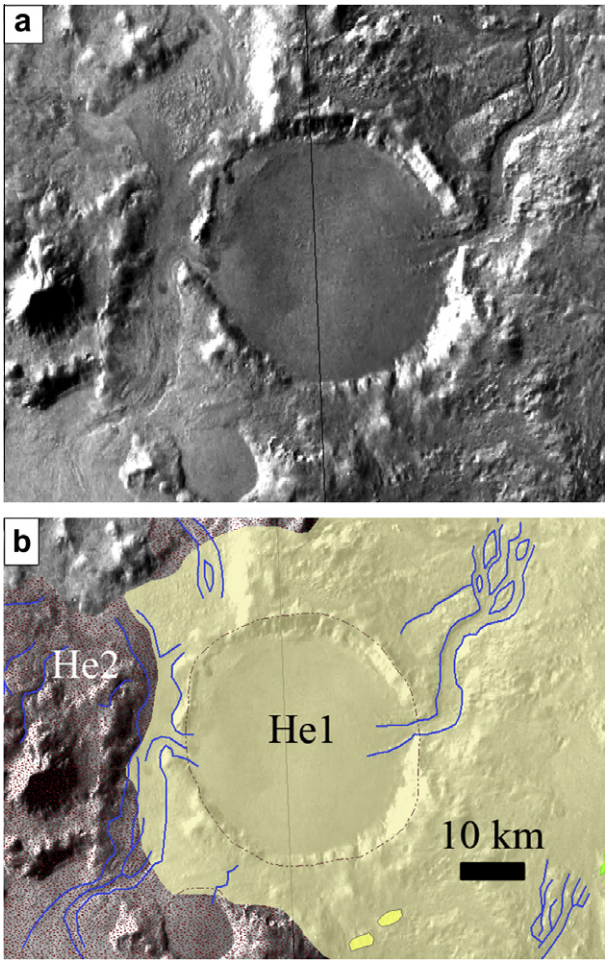

Fig. 5. *Ejecta-filled crater.* Just west of Hale, Hale ejecta breached the rim of a pre-existing crater, filled the crater, then flowed out the other side. The contact between He1 and He2 is approximate or gradational in many locations around the crater, particularly within Argre basin where the terrain is rough and mantling materials blanket much of the surface. Here the He1 unit has been extended across the crater because rough ejecta is visible on the other side. However, it is possible that He2 is found within the pre-existing crater as well. Fig. 5a shows what the region looks like in the THEMIS daytime-IR mosaic; Hale crater map units have been added to Fig. 5b. The images in this figure are a subset of the THEMIS daytime-IR mosaic used as base map.

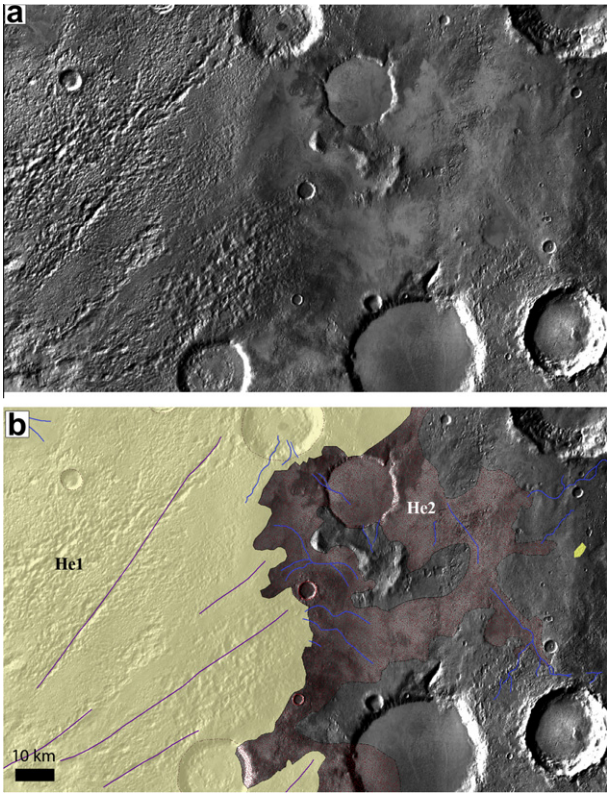

Fig. 6. *Northeastern ejecta.* The fluidized nature of He2 is clearly demonstrated in this image, where He2 appears to have flowed out of and away from the much rougher He1. The lines in He1 trace out a course texture within the unit, apparently defined by ballistic ejecta trajectories from Hale crater. Fig. 6a shows what the region looks like in the THEMIS daytime-IR mosaic; Hale crater map units have been added to Fig. 6b. The images in this figure are a subset of the THEMIS daytime-IR mosaic used as base map.

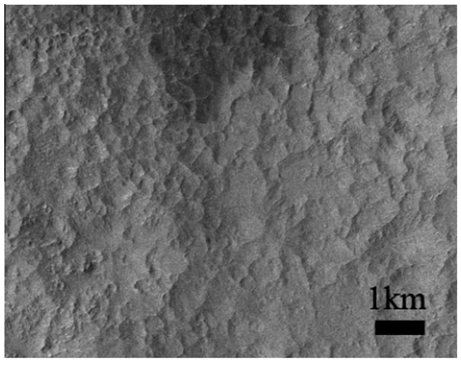

Fig. 7. *Ponded and pitted material (Pp).* The pitted floor northeast of Hale's central peak in CTX image P05_002787_1441_XN_35S036W. Pits are tens to hundreds of meters in diameter and are interpreted to be collapse pits, formed by volatiles escaping from a mixture of impact melt and lithic clasts. Image source: http://www.global-data.mars.asu.edu/bin/ctx.pl.

and longer channels have sinuous patterns. Most channels originate in the distal sections of He1 and throughout He2; several channels extend beyond the boundary of He2 and a few begin beyond this boundary. The channels are up to a few km across, though many are much smaller, and extend as far as 460 km from Hale's southwestern rim. Channels crudely radiate from Hale in all directions (though they are strongly influenced by local topography), but the highest concentration of channels is south–southwest of the crater, on the northern slope of Argyre basin (Fig. 2).

Short (<5 km), narrow (<0.5 km wide), straight chutes flanked by elevated banks are mapped as *raised-rim channels* (Fig. 9). Channels of this type are found on relatively steep slopes (~0.3°) along the slope break leading into Argyre basin and are interpreted as constructional, rather than erosional, built up by debris flows.

Prominent large channels or valleys that underlie, and therefore predate, Hale ejecta are mapped as *pre-existing channels or valleys (Pc)*. These depressions were utilized as conduits by Hale ejecta, transporting material farther from the primary cavity than would otherwise have been possible. For example, the He1 ejecta unit flows farther from Hale's primary crater in the Pc south of Hale crater than in adjacent areas outside the Pc (Fig. 2). The pre-existing channel north of Hale, overprinted by Bond and Holden craters, is Uzboi Vallis. Hale impacted what appears to be an extension of this channel, based on the proximity and the similar size, shape, and sinuosity of the channel and the valleys. The extension must exist in the hypothesis of Parker (1996) that a lake in Argyre basin overflowed into Uzboi Valles. The association of the Pc southeast of Hale with Uzboi and the valley segment northeast of Hale, between Hale and Bond craters, is clearest in the narrow section of trough directly south of Hale. The morphology of the features, including

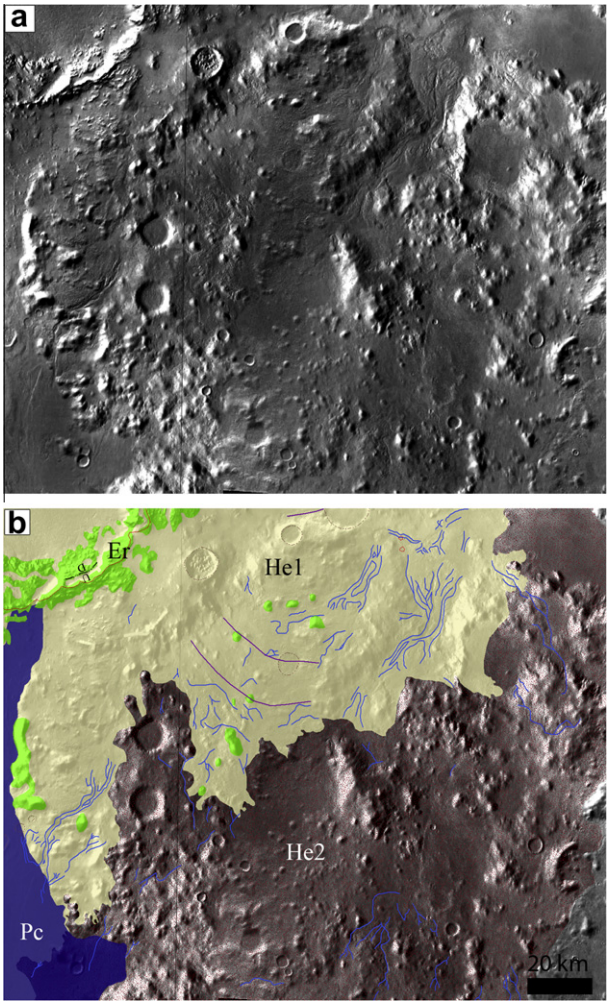

Fig. 8. *Southeastern channels.* A closer view of channels emanating from Hale ejecta. The spatial and temporal association between the channels and Hale's ejecta strongly suggest that the Hale-forming impact event also carved or modified the channels. In this location, the lines in He1 indicate what appears to have been the general direction of flow of the ejecta in this location. Fig. 8a shows what the region looks like in the THEMIS daytime-IR mosaic; Hale crater map units have been added to Fig. 8b. The images in this figure are a subset of the THEMIS daytime-IR mosaic used as base map.

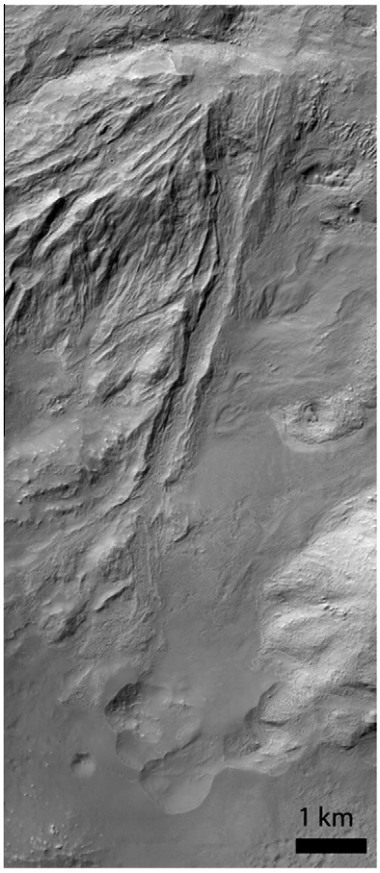

Fig. 9. *Debris flow.* HiRISE image (PSP_007033_1445) of a chute created by a debris flow. These channels are mapped as "raised-rim channels." HiRISE images used here and in Figs. 13 and 14 are available at http://www.hirise.lpl.arizona.edu/.

the trough diameters, is most similar in this location. The Pc continues southeast of Hale along the northeast margin of Argyre where it is the largest, most prominent, sinuous valley in the region.

3.6. Cross-section

A cross-section through Hale crater, drawn in the inferred direction of travel of the Hale-forming projectile (Fig. 10), is provided in Fig. 11. The elevation difference caused by the regional slope into Argyre is clear, as are differences in Hale's rimcrest elevation and terrace development (e.g. Melosh, 1989; Melosh and Ivanov, 1999) inside and outside Argyre basin. A series of listric normal faults is interpreted to underlie the rim terraces (e.g. Melosh, 1989; Melosh and Ivanov, 1999; Tornabene et al., 2008a,b). A smaller normal fault in Hale's southeast indicates a slump in the ejecta (e.g. Melosh and Ivanov, 1999). Material compressed during the initial stages of the impact event that rebounded to form the central peak complex is depicted with associated reverse faults (e.g. Kenkmann and Poelchau, 2009; Poelchau and Kenkmann, 2008). The complex faulting associated with the formation of Argyre basin

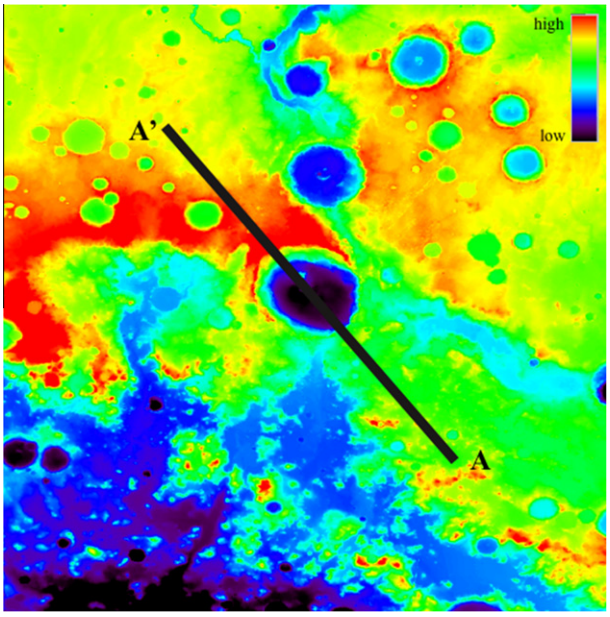

Fig. 10. *Cross-section location.* The cross-section through Hale crater is drawn in the inferred direction of travel of the Hale-forming bolide: from southeast to northwest. The elevation map highlights the elevation differences within and around Hale crater. Hale's northern rim crest is >3 km above the southern rim, and the difference in elevation within and outside of Argyre basin is also clearly illustrated.

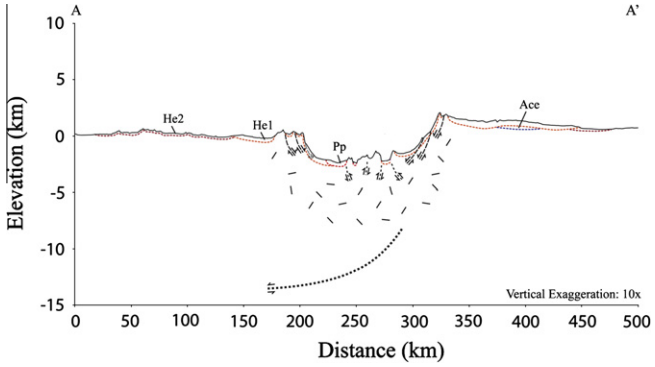

Fig. 11. *Cross-section through Hale crater.* The cross-section through Hale crater makes the uneven topography on which Hale crater formed more evident. The elevation difference associated with Argyre is clearly apparent, as is the difference in Hale's terrace development and rimcrest elevation inside and outside the basin. Normal faults are interpreted to have created rim terraces and a slump (small normal fault; on left) in the ejecta. Reverse faults are inferred to have been associated with uplifting the central peak complex. The complex faulting associated with the formation of Argyre basin is represented by a single large inferred fault at base of the cross-section. The pattern below Hale's primary crater depicts the fracturing of the bedrock caused by the impact. A topographic rise in He1 northwest of Hale is caused by another (unnamed) crater's ejecta (Ace) underlying Hale ejecta. The cross-section further emphasizes the abundance of He2 within the basin and the greater amount of He1 to the northwest. The topographic profile for the cross-section was extracted from a MOLA DEM. Actual depths of faults and fractures are unknown and approximated.

is schematically represented by a single large inferred fault at the base of the cross-section. The pattern below Hale's primary crater depicts the fractured bedrock caused by the impact (e.g. Melosh, 1989; Melosh and Ivanov, 1999). Actual depths of faults and fractures are unknown and approximated.

4. Streaks

A starburst pattern of relatively bright (warm) streaks in THEMIS nighttime IR images, indicating areas with relatively high thermal inertia and/or low albedo, radiates from Hale. These streaks can be several tens of km long and are typically 1–3 km wide. The most prominent streaks are shown in Fig. 12, but a hint of the pattern extends almost to Vallis Marineris, over 1000 km away. Many seem to originate at nighttime-IR-bright rims of smaller craters surrounding Hale, and some are slightly deflected around topographic obstacles such as large ($\geqslant$50 km) crater rims. A few

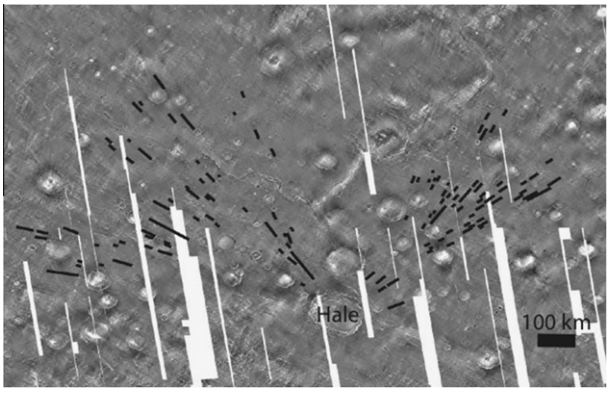

Fig. 12. *Hale streaks.* A pattern of bright streaks in THEMIS nighttime IR images radiates from Hale. The most prominent streaks are traced in this image, and a hint of this pattern extends almost to Vallis Marineris, over 1000 km away. Streaks can be several tens of kilometers long and are typically 1–3 km wide. These streaks may have been formed by a base surge associated with the Hale-forming impact event.

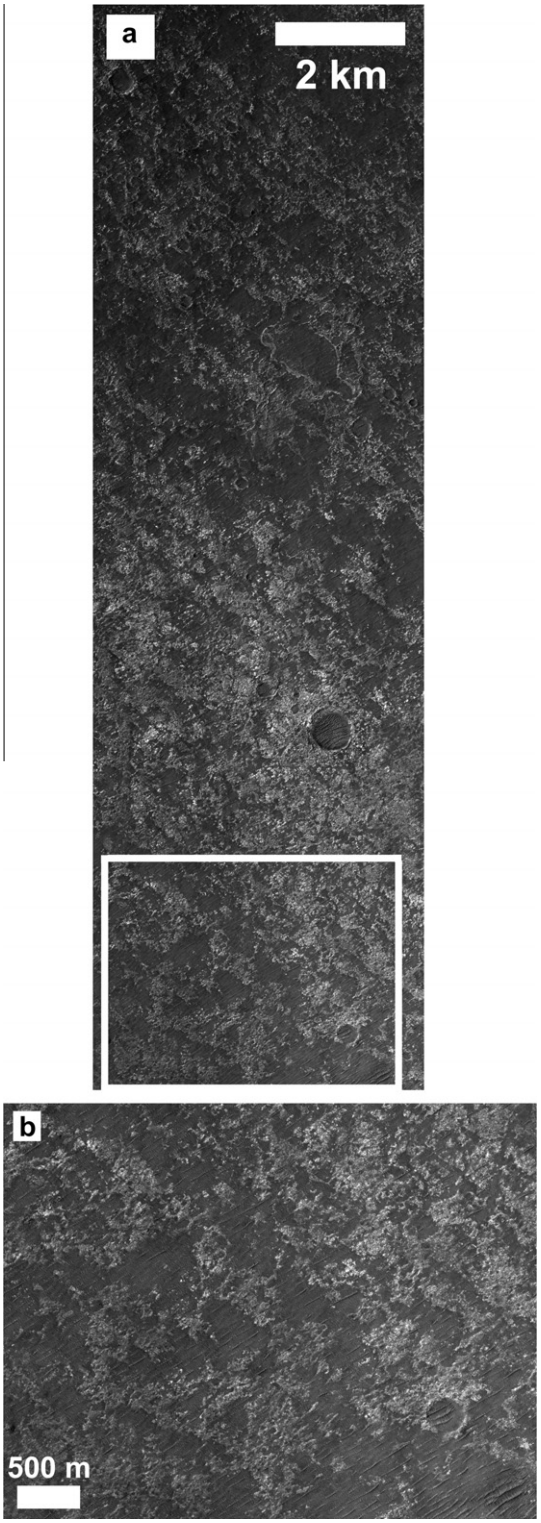

Fig. 13. *HiRISE image of a Hale streak.* a shows a portion of one of Hale's streaks captured in HiRISE image ESP_013916_1485. This image is not included in the subset of the entire mapping area included in Fig. 2 and 4; it is located northwest of Hale crater at 31.4°S, 314.0°E. b is a closer view of the streak; its location is outlined in white in a. Both images show bright scoured bedrock interlaid with darker aeolian deposits organized into linear dunes that are oriented perpendicular to the bedrock grooves. The aeolian material may have been initially emplaced by a base surge associated with the Hale-forming impact. The streaks may demonstrate the impactor's ability to mobilize aeolian materials even large distances (>10 radii) from the impact site. Hale crater is ~500 km to the bottom right of the images, and north is slightly left of the top.

streaks are co-linear with chains of Hale's secondary craters, but are not directly associated with obvious secondaries. The absence of a clear connection to secondary craters makes it difficult to determine whether these rays formed in the same manner as typical crater rays (Fielder, 1962; McEwen et al., 2005; Tornabene et al., 2006).

A portion of a streak captured in HiRISE image ESP_013916_1485 (Fig. 13a and b) reveals scoured bedrock with aeolian deposits partially filling depressions. The aeolian material is organized into linear dunes oriented perpendicular to the bedrock grooves (Fig. 13b). These materials may have been initially emplaced by a base surge or air-blast associated with the Hale-forming impact event, which could have collected and concentrated unconsolidated surficial material. The unconsolidated aeolian materials would later have been reworked, thus the linear dunes are likely not original features.

5. Volume of water mobilized by Hale-forming impact

5.1. Discharge estimates

To estimate the volume of fluid mobilized by the Hale-forming impact, which carved or modified the channels discussed above, we used a DEM constructed from the HiRISE stereo pair PSP_005609_1470 and PSP_005754_1470 using techniques described by Kirk et al. (2008). Although the channels in this DEM are relatively small, the exceptional resolution provided by HiRISE imagery allows detailed analysis of their dimensions. Although MOLA is another source of topographic data, its footprints are too widely spaced (300 m along-track, up to 4 km across-track; Smith et al., 2001) to obtain profiles of Hale's channels in sufficient detail for fluid volume estimates.

We calculated peak flow velocities in four of Hale's channels (shown in Fig. 14) using the Manning and Darcy–Weisbach equations, and multiplied these values by channel cross-sectional areas to estimate peak discharges. Although intended for use with steady, uniform flow (e.g. Silberman et al., 1963; O'Connor and Webb, 1988), these equations have been applied to catastrophic flows on Mars in many previous studies (e.g. Carr, 1979; Komatsu and Baker, 1997; Grant and Parker, 2002; Wilson et al., 2004; Kleinhans, 2005; Leask et al., 2006). Their accuracy may be limited outside of their intended application, but we used versions of these equations specifically adapted for martian conditions to ensure the flow estimates were as accurate as possible.

Given the difficulty of modeling slurries and the unknown properties of the flows that carved Hale's channels, we initially estimated flow within channels assuming they were carved by pure water. We then adjusted our velocity and discharge estimates for the more likely scenario that the channels were carved by a slushy mixture of water-rich debris by assuming the water content was 40%. We select this value because the braided morphology of Hale's channels indicate they were carved by flows with a high sediment content, and 40% is an approximate minimum water content required to make material flow like a low-viscosity liquid (Rodine and Johnson, 1976; Iverson et al., 1997).

Channel slopes and cross-sections (Fig. 15) were extracted from the HiRISE DEM using RiverTools (RIVIX, 2005). (Multiple cross-sections were taken of each channel, but only the profiles used in the analysis are traced in Fig. 15.) To correct for DEM pixelation and noise, we smoothed the profiles before determining cross-sectional areas. We assumed channel-full flow, resulting in estimates of peak flow velocity and peak discharge.

The HiRISE DEM reveals nested sub-channels within the channels in our study. The main channels may have been carved as a result of the Hale-forming impact, or they may have been pre-existing features that were modified by this impact event. Decreasing flow over time could have produced the sub-channel terraces: as the water supply dwindled, smaller channels may have been carved into floors of larger channels. Pulses of flow could also have produced terraces: a delayed release of water from melting ice within or beneath hot ejecta may have followed an initial burst of liquid from the heat of the impact.

The cross-sectional shapes of the channels (particularly the elevations of the channel floors) may have also changed over time, complicating discharge estimates from the larger, higher sub-channels. Discharge from the Hale-forming impact formed at least the lowest, but possibly all of the terraced sub-channels. We estimated flow velocities and discharges for the three topographically lowest terrace levels within each channel.

5.1.1. The Manning equation

The simplicity of the Manning equation makes it a popular tool for calculating discharge. The original form of the equation (Manning, 1891) is

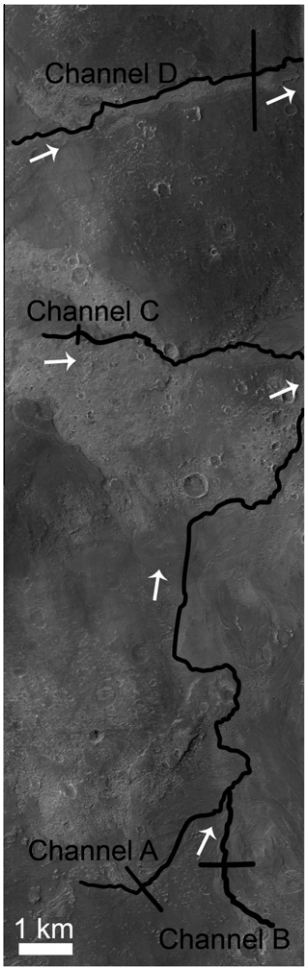

Fig. 14. *HiRISE image of Hale channels.* Sections of some of Hale's small channels found near the edge of He2, northwest of Hale crater (see Fig. 4 for image location) are captured in HiRISE image PSP_005609_1470. This image and its stereo pair (PSP_005754_1470) were used to construct a digital elevation model (DEM) of the channels so that they could be used for flow and discharge calculations (see text). Discharge estimates from channels A through D were used to estimate the volume of water mobilized or released by the Hale-forming impact. Several profiles were taken of each channel; the locations of the profiles selected for this study are indicated. White arrows indicate the downslope direction. North is to the top right of the image.

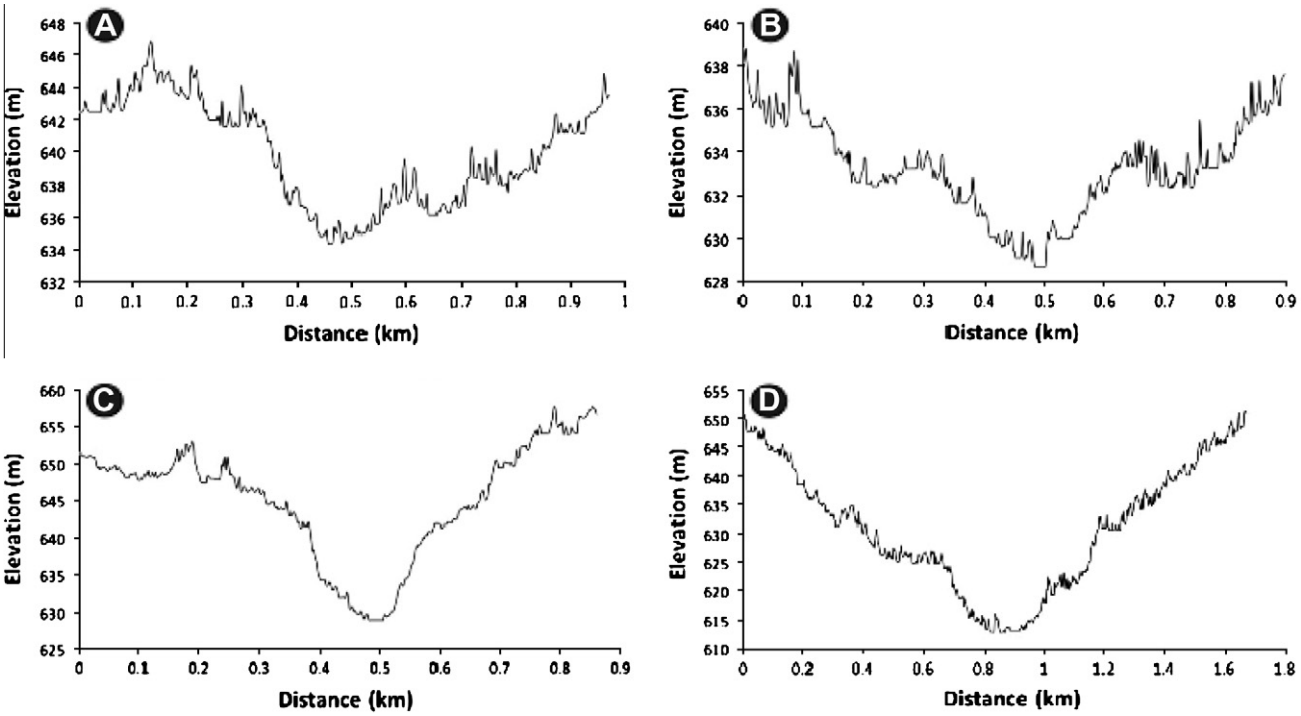

Fig. 15. *Channel profiles*. Representative cross-sections through four channels in the HiRISE DEM constructed from the stereo pair PSP_005609_1470 and PSP_005754_1470. These profiles are original data from the DEM, before they were smoothed. Note that the profiles do not all have the same scale.

$$U_c = \frac{(R^{2/3}S^{1/2})}{n}, \tag{1}$$

where U_c is the mean water flow velocity (m s^{-1}) in the channel, R is the hydraulic radius of the channel (m), S is the energy slope of the flow, and n is the Manning coefficient. S can be approximated as the channel bed surface slope (Silberman et al., 1963). In its most precise form, R is defined as the cross-sectional area divided by the wetted channel perimeter. It can be approximated as

$$R = \frac{Wd}{W + 2d} \tag{2}$$

where W is the channel width (m) and d is the mean depth of water in the channel (m). However, in channels where W is considerably larger than d, as is the case for most natural channels, $R \approx d$ (Wilson et al., 2004). We used this simplification in our calculations.

Discharge, Q, is

$$Q = U_c A, \tag{3}$$

where A is the cross-sectional area of the channel (m^2).

The Manning coefficient is intended for terrestrial applications; transferring it to other planets or satellites without considering differences in the acceleration due to gravity (g) can lead to errors. Wilson et al. (2004) calculated $n = 0.0545$ s m$^{-1/3}$ for martian channels, accounting for martian g as well as typical channel roughness. We adopted this value of n for our discharge calculations.

5.1.2. The Darcy–Weisbach equation

The Darcy–Weisbach equation has been promoted for extraterrestrial geomorphologic calculations due to (1) its empirically determined, dimensionless friction coefficient, useful when comparing flows of different scales in different gravitational regimes (Wilson et al., 2004); and (2) its incorporation of depth-dependent roughness, as opposed to constant roughness assumed by the Manning equation (Kleinhans, 2005). The Darcy–Weisbach equation is:

$$U_c = \left(\frac{8gRS}{f_c}\right)^{1/2}, \tag{4}$$

where g is the acceleration due to gravity (3.74 m s^{-2} on Mars) and f_c is the friction factor. To calculate flow velocities for the channels near Hale, we used friction factors from Wilson et al. (2004) for upper regime sand bed channels (URSBCs) and gravel bed channels (GBCs). For URSBCs,

$$\left(\frac{8}{f_c}\right)^{1/2} = 7.515\left(\frac{R}{D_{50}}\right)^{0.1005} S^{0.03953}\sigma_g^{-0.1283}, \tag{5}$$

where D_{50} is the median channel bed clast size and σ_g is the geometric standard deviation of the bed clast size distribution. For GBCs,

$$\left(\frac{8}{f_c}\right)^{1/2} = 5.75\log_{10}\left(\frac{aR}{3.5D_{84}}\right), \tag{6}$$

where

$$a = 11.1\left(\frac{R}{d_m}\right)^{-0.314}, \tag{7}$$

D_{84} is the channel bed clast size such that 84% of the clasts are smaller than D_{84}, and d_m is the maximum depth of the channel. We assumed $\sigma_g = 2.9$ based on grain size data at the Viking 1, Viking 2, and Pathfinder landing sites, reported by Wilson et al. (2004) from data in Golombek and Rapp (1997) and Golombek et al. (2003). We used values assumed by Kleinhans (2005) for D_{50} and D_{84}: 0.1 m and 0.6 m, respectively.

5.1.3. Results

Results of flow velocity and discharge calculations are in Table 1. Terrace levels are reported as 1, 2, and 3, with increasing height above the channel floor, within channels A, B, C, and D. Calculated average peak flow velocity in the sub-channels is 8.2 m s^{-1} using the Manning equation, 7.2 m s^{-1} for URSBC, and 5.9 m s^{-1} for GBC (Fig. 16). The highest calculated flow velocity is 19.2 m s^{-1}

Table 1
Flow velocity and discharge estimates for representative channels. Discharge estimates for representative channels using Manning (M) and Darcy–Weisbach (D–W) equations, with friction factors for upper regime sand bed channels (URSBCs) and gravel bed channels (GBCs) for D–W. Sub-channels 1–3 correspond to their respective terrace levels within channels A–D. Other terms in table: hydraulic radius of channel, approximately equal to mean water depth (R); energy slope of the flow, approximated as channel bed surface slope (S); cross-sectional area of the channel (A); maximum depth of the channel (d_m); mean water flow velocity (U_c); and discharge (Q).

Sub-channel	R, m	S	A, m^2	d_m, m	U_c, m s^{-1}; M	U_c, m s^{-1}; D–W URSBC	U_c, m s^{-1}; D–W GBC	Q, m^3 s^{-1}; M	Q, m^3 s^{-1}; D–W URSBC	Q, m^3 s^{-1}; D–W GBC
A1	3.2	0.0022	450	12.09	1.9	1.9	1.2	850	870	530
A2	4	0.0022	770	11.91	2.2	2.2	1.4	1.7×10^3	1.7×10^3	1.1×10^3
A3	7.2	0.0022	3150	11.56	3.2	3.2	2.3	1.0×10^4	9.9×10^3	7.1×10^3
B1	1.2	0.0025	60	11.78	1.0	1.1	0.5	70	70	30
B2	4.6	0.0025	770	11.1	2.5	2.5	1.7	1.9×10^3	1.9×10^3	1.3×10^3
B3	7.2	0.0025	2530	11.1	3.4	3.3	2.4	8.6×10^3	8.3×10^3	6.0×10^3
C1	6	0.0232	520	11.1	9.2	8.3	6.2	4.8×10^3	4.3×10^3	3.2×10^3
C2	13	0.0232	1700	11.1	15.4	13.2	11.2	2.6×10^4	2.2×10^4	1.9×10^4
C3	18	0.0232	3300	11.1	19.2	16.0	14.2	6.3×10^4	5.3×10^4	4.7×10^4
D1	8	0.018	1760	11.1	9.8	8.8	6.9	1.7×10^4	1.5×10^4	1.2×10^4
D2	13	0.018	3880	11.1	13.6	11.7	9.9	5.3×10^4	4.5×10^4	3.8×10^4
D3	18	0.018	7480	11.1	16.9	14.2	12.5	1.3×10^5	1.1×10^5	9.4×10^4
AVG:	8.6	0.0115	2200	11.3	8.2	7.2	5.9	2.6×10^4	2.3×10^4	1.9×10^4

(C3, Manning equation) and the lowest calculated flow velocity is 0.5 m s^{-1} (B1, GBC). The average peak discharge for the sub-channels is 2.6×10^4 m^3 s^{-1} for the Manning equation, 2.3×10^4 m^3 s^{-1} for URSBC, and 1.9×10^4 m^3 s^{-1} for GBC (Fig. 17). The maximum peak discharge is 1.3×10^5 m^3 s^{-1} (D3, Manning) and the minimum is 30 m^3 s^{-1} (B1, GBC).

The flow velocities from the three equations cluster fairly well at flow velocities <~5 m s^{-1}. At higher velocities, the Manning equation yields the highest values and the Darcy–Weisbach GBC returns the lowest.

If we assume the duration of flow in Hale's channels was one week (6.0×10^5 s) to one month (2.6×10^6 s) and the slurry that carved the channels was 40% water, using a triangular hydrograph, the total volume of water that flowed through the channels in the HiRISE DEM at average peak discharge (2.3×10^4 m^3 s^{-1}) is 2.8×10^9 m^3 (one week) and 1.2×10^{10} m^3 (one month).

These volumes may be higher than the volumes required to form the channels because at the calculated velocities, unit power (mean velocity times bed shear stress) would be sufficiently high to cause considerable bed erosion on relatively short time scales. Peak flow durations of weeks would not be necessary to produce the measured channel dimensions.

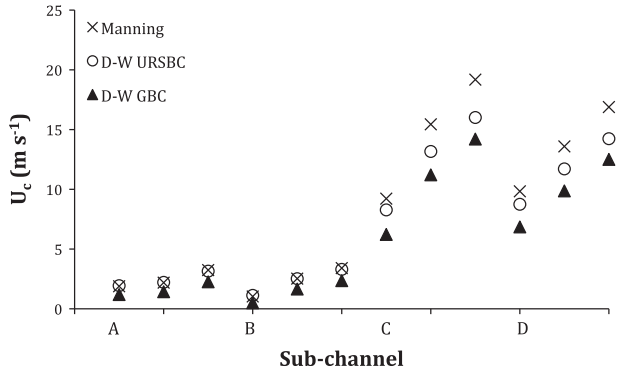

Fig. 16. *Estimates of flow velocities within Hale channels*. Flow velocities for Hale's channels A–D, for terrace levels 1–3 (topographically lowest to highest, depicted from left to right, respectively).

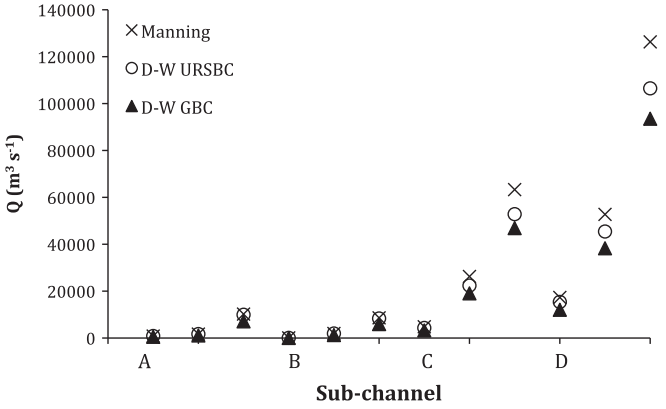

Fig. 17. *Discharge estimates for Hale channels*. Estimates of discharge in Hale's channels A–D, for terrace levels 1–3 (topographically lowest to highest, depicted from left to right, respectively).

6. Age of Hale

In order to constrain the age of the Hale impact event, we conducted a crater count of the interior of Hale's primary cavity, excluding areas of exposed rock, heavily pitted surfaces, gully deposits, and thick deposits of dust or sand. Roughly (to nearly perfectly) circular depressions surrounded by raised rims were identified as impact craters. Visible ejecta blankets surrounding some craters helped confirm their impact origin.

In the pitted terrain of Hale's interior, it was important to be able to distinguish impact craters from collapse pits. Besides the presence or absence of raised rims, we looked at the locations and arrangements of depressions to determine their classification. Pits are arranged into fairly regular patterns (e.g. pits of similar size are often adjacent, the largest pits are found towards the center of the crater, Bray et al., 2009), while impact craters are scattered at random. Circular depressions with raised rims superposed on interlocking pits were therefore identified as impact craters. Additionally, several impact craters appeared to have steeper slopes than the pits, resulting in a more striking contrast between comparatively darker shadows next to brighter slopes within impact craters than what was found in most collapse pits.

The craters visible in 6 m $pixel^{-1}$ CTX images in an 8117 km^2 area (Fig. 18) yielded a crater-retention age of 1 Ga (early to middle Amazonian), via the model of Hartmann (2005), for the largest craters in our count (Fig. 19). This is younger than the estimate of late Hesperian–early Amazonian by Cabrol et al. (2001). Two craters with diameters larger than 2 km were found in the counting area, which corresponds with a Lower Amazonian age in Tanaka (1986) [$N(2) = 250$]. 1 Ga is thus the minimum age of Hale.

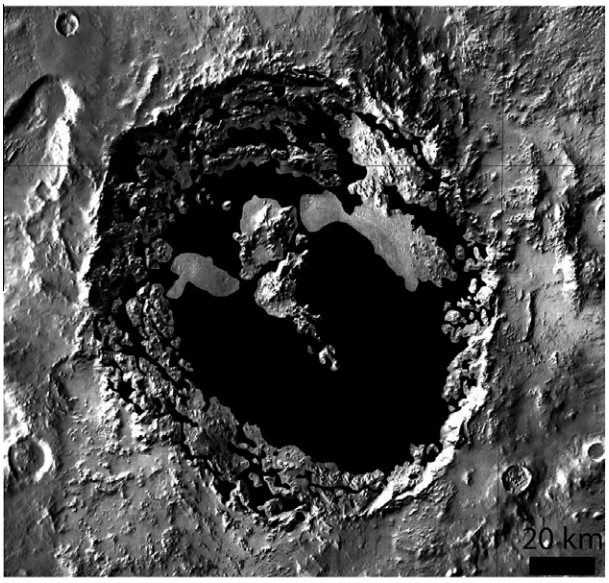

Fig. 18. *Crater count area.* We counted all of the craters within Hale's primary cavity visible in 6 m pixel^{-1} CTX images in an 8117 km^2 area. This area (shown in black) excludes exposed rock, gully deposits, thick deposits of dust or sand, and some heavily pitted surfaces. Crater count area is displayed on a THEMIS daytime-IR mosaic.

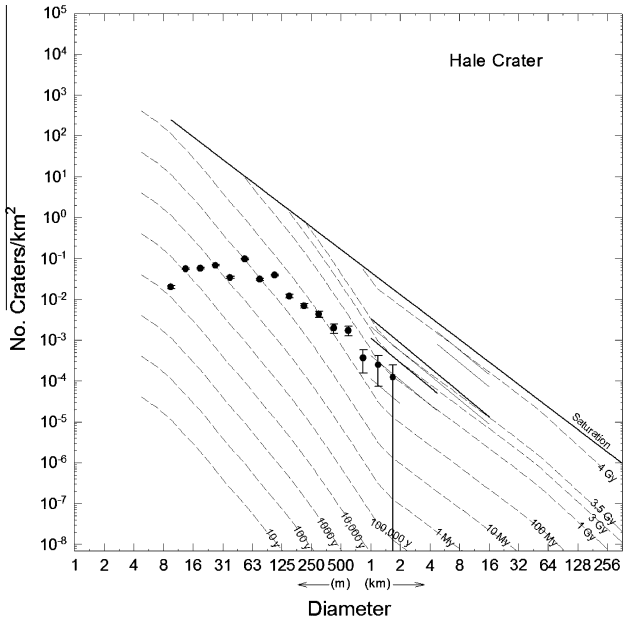

Fig. 19. *Crater count plot.* The plot of craters found within Hale's primary cavity yields a crater-retention age of 1 Ga, or early to middle Amazonian. This is a minimum age for Hale. A roll-over at smaller crater diameters may be due to degradation of smaller craters. Larger craters are more likely to be preserved and counted, so the age they yield is more likely to be accurate.

The slope of the crater-count plot is less steep than expected for the production function (e.g. Hartmann, 2005), with a roll-over at smaller crater diameters; more small craters are expected than we observe. The smaller craters may have been preferentially eroded, modified, or filled. Our count was conservative, only including obvious impact craters, which may have excluded some small impact craters, indistinguishable from pits. Larger craters are more likely to be preserved and counted, so the age they yield is more likely to be accurate.

7. Discussion

Portions of the martian crust are and/or were rich in water ice (e.g. Squyres, 1988; Mellon et al., 1997, 2004; Baker, 2001; Boynton et al., 2002; McEwen et al., 2007b; Senft and Stewart, 2008; Smith, 2009; Clifford et al., 2010), and heat generated by large impacts should melt subsurface ice (Stewart and Ahrens, 2005), creating surface runoff that could modify the surrounding terrain (e.g. Carr, 1996; Maxwell et al., 1973; Tornabene et al., 2007b; Williams and Malin, 2008; Morgan and Head, 2009). Hale crater and its associated channels support this hypothesis.

The channels carved or modified by Hale appear to emanate from and to have transported Hale ejecta, implying that the channels are original features in the ejecta, formed immediately after the Hale-forming impact event. The immature drainage pattern of the channels suggests the channel-forming event was brief, ending when source water was depleted or frozen.

Much of the melted ice excavated by the impact would likely have remained in the pore space of the ejecta. Water would only have been released from the ejecta to incise channels once the storage capacity of the ejecta pore space had been exceeded: i.e. the ejecta became over-saturated. The volume of water that exceeded the pore space of the ejecta could have contributed to channel incision.

7.1. Origin of the water

Given our estimate that $\sim 10^{10}$ m^3 of water formed some of Hale's smaller channels, we now consider possible origins of this water, e.g. subsurface ice, surficial ice, rainfall, hot springs, or an ice-rich impactor.

Clifford et al. (2010) reported evidence suggesting that the permafrost zone (that could be filled with ground ice) may extend to a depth of ~15 km at Hale's latitude. Other researchers also support an ice-rich martian crust (e.g. Squyres, 1988; Mellon et al., 1997, 2004; Baker, 2001; Boynton et al., 2002; McEwen et al., 2007b; Senft and Stewart, 2008; Smith, 2009; Clifford et al., 2010). To find out whether subsurface ice could supply enough water to carve Hale's channels, we first consider the amount of water that could have been released by the Hale-forming impact from water ice in the subsurface pore space. We assume 10% porosity, based on a conservative estimate of the available pore space in the upper 1–2 km of the martian subsurface (MacKinnon and Tanaka, 1989). To estimate the volume of material excavated by the Hale-forming impact, we project an approximate pre-impact surface along the cross-section line (Fig. 11) and integrate the volume of the space between this line and the crater floor. We obtain an average crater volume of 1.9×10^{13} m^3, which is approximately equal to the ejecta volume in this large complex crater (Melosh, 1989). If 10% of this volume was water ice, 1.9×10^{12} m^3 of liquid water could have been excavated, with some fraction of this water mobilized to form the channels and fluidized ejecta patterns associated with Hale crater.

It is unlikely that all of this ice volume would have melted upon impact: some of the ice would have vaporized during the impact and some ice in areas that experienced low shock pressures and temperatures during the impact event may have remained solid, until possible later melting due to proximity to hot ejecta. However, the water produced by melting this volume of ice is orders of magnitude greater than our estimated amount of water required to form the channels, making subsurface ice a sufficient source of water to form or modify Hale's channels and to produce the fluidized ejecta patterns surrounding Hale crater.

If the 200,000 km^2 area covered by Hale ejecta outside of Hale's primary crater contributed additional water from ice melting be-

neath the relatively hot ejecta blanket (e.g. Newsom et al., 1986), even more water would have been available. If an average thickness of 5 m of permafrost (at 10% ice by volume) were melted below He1 and He2, an additional 1.0×10^{11} m^3 water could have been released to carve channels surrounding Hale. But considering the amount of water that could have melted beneath both of Hale's ejecta units may lead to an overestimate. Water released from within and beneath He1 likely carved or modified the channels and provided the volatiles for He2, so we next estimate the amount of water that could have melted from permafrost beneath He1 outside of Hale crater (an 80,000 km^2 area) and obtain a value of 4.0×10^{10} m^3 of water. This volume of water would be sufficient to carve the small Hale channels analyzed in this study; if added the melted ice within Hale's ejecta, this water could potentially have contributed to carving or modifying larger channels.

Surficial ice could have provided enough water to carve small Hale channels if the entire ~95,000 km^2 area blanketed by He1 was covered with 1 m of pure ice, perhaps covered by a sublimation lag deposit, at the time of impact. If all of this surficial ice was melted and incorporated into the ejecta, $\sim 8.7 \times 10^{10}$ m^3 of liquid water would be available for fluidizing ejecta and carving channels, only enough to carve the small channels in the HiRISE DEM, and likely not enough to form or modify the larger channels associated with Hale.

The average peak discharges for Hale's small sub-channels correlate well with the largest estimated peak discharges in channels associated with Sinton crater ($2.5 \times 10^4 - 1.4 \times 10^5$ m^3 s^{-1}), a 60-km-diameter impact crater in the Deuteronilus Mensae region of the dichotomy boundary (Morgan and Head, 2009). Melted surficial ice could produce channels surrounding Sinton crater because of the very thick (0.5–1 km) deposit of ice hypothesized to have been present in the area at the time of impact (Morgan and Head, 2009). If Argyre was experiencing a period of glaciation (e.g. Kargel and Strom, 1992; Baker, 2001; Banks et al., 2008) when Hale crater formed, with ice deposits of similar thickness at the impact site, melted surficial ice or snow could have contributed to sculpting Hale's channels.

Current near-surface temperatures and pressures in the area are well below those that would support liquid water or ice at the surface (Christensen et al., 1998; Conrath et al., 2000; Carr, 2006). It is possible that they may have been stable at the time of Hale's formation, and hydrated minerals may also have been present and supplemented water contributions, but these sources are not sufficient to explain the fluidized morphologies surrounding Hale.

Other possible sources of water are less likely to have produced the fluvial features surrounding Hale crater. We rule out rainfall for several reasons. (1) Hale's channels are fairly immature. They do not converge downstream into higher-order systems in a manner typical of pluvial drainages (e.g. Morgan and Head, 2009). (2) There is no evidence of channels at high elevations. If rainwater sculpted Hale's channels, tributaries should be found on elevated slopes (e.g. Williams and Malin, 2008), such as the crater rim. (3) Any impact-generated rainfall should have been concentrated in Hale's primary cavity, yet it lacks well-developed channels at map scale. (4) The discharge rates determined for even small Hale channels seem most probably to have been much larger than would be generated by precipitation (e.g. Fassett and Head, 2005; Morgan and Head, 2009). (5) Rainfall would not have produced the fluidized ejecta morphologies surrounding Hale. If there was rain, it must have been supplemented by another source of water.

The absence of channels within or near the primary cavity also weakens the hypothesis for a sustained impact-induced hydrothermal system as a water source. Impact-generated hot springs should occur along faults, such as the listric faults of the crater rim (e.g. Osinski et al., 2005), yet channels do not begin for some distance from the primary cavity.

Impact by a comet is unlikely to account for Hale's muddy ejecta, even if the comet were entirely water ice. An impactor is typically 5–10% the diameter of its resulting crater (Melosh, 1989) and <1% of the impactor's volume is typically incorporated into the ejecta (Koeberl, 1998). A comet would incorporate less of its volume into ejecta than most other bolides because of its high volatile content and high impact velocity; most of a comet would vaporize during impact. A pure-water–ice comet 10% the diameter of Hale (~14 km) would have a volume of $\sim 2.7 \times 10^{12}$ m^3. 0.1% of this volume (an equivalent of 2.5×10^9 m^3 of liquid water) would be insufficient to form even the small channels in the HiRISE DEM, much less the larger channels and fluidized ejecta features surrounding Hale.

The Hale-forming impactor may have struck a particularly volatile-rich area near Uzboi Vallis. There is no evidence that Hale crater ever filled with water or other fluids, so ULM is unlikely to have been active at the time of impact. However, water once flowed across the surface here, and there may have been a locally thicker ice layer when Hale formed. Because of the lack of evidence for rainfall or hot springs, the insufficient water contributions of a comet, the instability of subsurface water or surficial snow or ice, and the likely abundance of subsurface ice, subsurface ice remains the most plausible water source for the fluvial morphologies surrounding Hale.

7.2. Implications

The presence of channels does not necessarily indicate a warmer, wetter global climate when the channels were active (e.g. Brakenridge et al., 1985; Cabrol et al., 2001; McEwen et al., 2007b). Hale's channels formed when a bolide struck a location rich with subsurface volatiles, Sinton's channels may have resulted from an impact into thick surficial ice deposits (Morgan and Head, 2009), and other martian craters that formed in volatile-rich locations may also have had channel systems associated with them.

The number, size, and extent of the channels created as a result of the Hale-forming impact are substantial. If channels commonly form in response to large impact events, water mobilized by many such events during enhanced bombardment early in martian history may help explain the presence of valley networks, phyllosilicates, and denuded terrain characteristic of Noachian landscapes (e.g. McEwen et al., 2007b; Tornabene et al., 2007b).

8. Conclusions

Hale is surrounded by an impact-generated and/or impact-modified channel system, resulting from between 10^{10} and 10^{12} m^3 of liquid water mobilized by the Hale-forming impact. This quantity of water most likely came from impact-caused melting of subsurface ice, and is consistent with 10% of Hale's ejecta by volume being water ice. We determined a 1 Ga minimum age for Hale, at which time the surface and/or subsurface at the impact site must have been water–ice-rich. Hale crater demonstrates the role impact craters may have played in supplying enough water to the martian surface to fluvially modify the landscape, particularly during the higher cratering rate early in martian history, without invoking a long-lived wetter climate or thicker atmosphere.

Acknowledgments

We thank the MRO Project, HiRISE Science Team and the staff at the HiRISE Operations Center for making this research possible. We also thank the Planetary Science Institute, particularly Mary Bourke, for the use of computing facilities. Comments from Kevin Jones and three anonymous reviewers improved this manuscript. This

work was funded by the NASA Mars Reconnaissance Orbiter and Mars Data Analysis projects.

References

Baker, V.R., 1980. Nirgal Vallis. Rep. Planet. Geol. Program – 1980, 345–347.

Baker, V.R., 2001. Water and the martian landscape. Nature 412, 228–236.

Banks, M.E. et al., 2008. High Resolution Imaging Science Experiment (HiRISE) observations of glacial and periglacial morphologies in the circum – Argyre Planitia highlands, Mars. J. Geophys. Res. 113, E12015.

Barlow, N.G., Bradley, T.L., 1990. Martian impact craters: Correlations of ejecta and interior morphologies with diameter, latitude, and terrain. Icarus 87, 156–179.

Barlow, N.G., Boyce, J.M., Costard, F.M., Craddock, R.A., Garvin, J.B., Sakimoto, S.E.H., Kuzmin, R.O., Roddy, D.J., Soderblom, L.A., 2000. Standardizing the nomenclature of martian impact crater ejecta morphologies. J. Geophys. Res. 105, E11.

Boyce, J.M., Mouginis-Mark, P.J., 2006. Martian craters viewed by the Thermal Emission Imaging System instrument: Double-layered ejecta craters. J. Geophys. Res. 111, E10005.

Boynton, W.V. et al., 2002. Distribution of hydrogen in the near surface of Mars: Evidence for subsurface ice deposits. Science 297 (5578), 81–85.

Brakenridge, G.R., Newsom, H.E., Baker, V.R., 1985. Ancient hot springs on Mars: Origins and paleoenvironmental significance of small martian valleys. Geology 13 (12), 859–862.

Bray, V.J., Tornabene, L.L., McEwen, A.S., Mattson, S.S., 2009. Measurement of small-scale pits in the Corinito crater, Mars. Lunar Planet. Sci. XXXX, 1389.

Cabrol, N.A., Wynn-Williams, D.D., Crawford, D.A., Grin, E.A., 2001. Recent aqueous environments in martian impact craters: An astrobiological perspective. Icarus 154, 98–112.

Carr, M.H., 1979. Formation of martian flood features by release of water from confined aquifers. J. Geophys. Res. 84 (B6), 2995–3007.

Carr, M.H., 1996. Water on Mars. Oxford Univ. Press, New York, NY.

Carr, M.H., 2006. The Surface of Mars. Cambridge University Press, Cambridge, UK.

Christensen, P.R. et al., 1998. Results from the Mars Global Surveyor Thermal Emission Spectrometer. Science 279, 1692–1698.

Christensen, P.R. et al., 2004. The Thermal Emission Imaging System (THEMIS) for the Mars 2001 Odyssey Mission. Space Sci. Rev. 110 (1/2), 85–130.

Clifford, S.M., Lasue, J., Heggy, E., Boisson, J., McGovern, P., Max, M.D., 2010. Depth of the martian cryosphere: Revised estimates and implications for the existence and detection of subpermafrost groundwater. J. Geophys. Res. 115, E07001.

Conrath, B.J., Pearl, J.C., Smith, M.D., Maguire, W.C., Christensen, P.R., Dason, S., Kaelberer, M.S., 2000. Mars Global Surveyor Thermal Emission Spectrometer (TES) observations: Atmospheric temperatures during aerobraking and science phasing. J. Geophys. Res. 105 (E4), 9509–9519.

Fassett, C.I., Head III, J.W., 2005. Fluvial sedimentary deposits on Mars: Ancient deltas in a crater lake in the Nili Fossae region. Geophys. Res. Lett. 32, L14201.

Fielder, G., 1962. Ray elements and secondary-impact craters on the Moon. Astrophys. J. 135, 632.

Golombek, M., Rapp, D., 1997. Size-frequency distribution of rocks on Mars and Earth analog sites: Implications for future landed missions. J. Geophys. Res. 102 (E2), 4117–4129.

Golombek, M.P., Haldermann, A.F.C., Forsberg-Taylor, N.K., DiMaggio, E.N., Schroeder, R.D., Jakosky, B.M., Mellon, M.T., Matijevik, J.R., 2003. Rock size-frequency distributions on Mars and implications for Mars Exploration Rover landing safety and operations. J. Geophys. Res. 108 (E12), 8086.

Grant, J.A., Parker, T.J., 2002. Drainage evolution of the Margaritifer Sinus region, Mars. J. Geophys. Res. 107 (E9), 5066.

Grant, J.A., Buczkowski, D., Irwin, R.P. III, Siebach, K., 2010. A lake in Uzboi Vallis and implications for late Noachian climate on Mars. Lunar Planet. Sci. XXXXI, 1834.

Hartmann, W.K., 2005. Martian cratering. 8: Isochron refinement and the chronology of Mars. Icarus 174, 294–320.

Herrick, R.R., Hessen, K., 2006. The planforms of low-angle impact craters in the northern hemisphere of Mars. Meteorit. Planet. Sci. 41 (10), 1483–1495.

Iverson, R.M., Reid, M.E., LaHusen, R.G., 1997. Debris-flow mobilization from landslides. Annu. Rev. Earth Planet. Sci. 25, 85–138.

Jaumann, R., Reiss, D., 2002. Nirgal Vallis: Evidence for extensive sapping. Lunar Planet. Sci. XXXIII, 1579.

Kargel, J.S., Strom, R.G., 1992. Ancient glaciation on Mars. Geology 20, 3–7.

Kenkmann, T., Poelchau, M.H., 2009. Low-angle collision with Earth: The elliptical impact crater Matt Wilson, NT, Australia. Geology 37, 459–462.

Kirk, R.L. et al., 2008. Ultrahigh resolution topographic mapping of Mars with MRO HiRISE stereo images: Meter-scale slopes of candidate Phoenix landing sites. J. Geophys. Res. 113, E00A24.

Kleinhans, M.G., 2005. Flow discharge and sediment transport models for estimating a minimum timescale of hydrological activity and channel and delta formation on Mars. J. Geophys. Res. 110, E12003.

Koeberl, C., 1998. Identification of meteoritic components in impactites. Geol. Soc., Lond., Spec. Publ. 140, 133–153.

Kolb, K.J., Pelletier, J.D., McEwen, A.S., and HiRISE Team, 2010. Modeling the formation of bright slope deposits associated with gullies in Hale Crater, Mars: Implications for recent liquid water. Icarus 205, 113–137.

Komatsu, G., Baker, V.R., 1997. Paleohydrology and flood geomorphology of Ares Vallis. J. Geophys. Res. 102 (E2), 4151–4160.

Leask, H.J., Wilson, L., Mitchell, K.L., 2006. Formation of Ravi Vallis outflow channel, Mars: Morphological development, water discharge, and duration estimates. J. Geophys. Res. 111, E08070.

MacKinnon, D.J., Tanaka, K.L., 1989. The impacted martian crust: Structure, hydrology, and some geologic implications. J. Geophys. Res. 94 (B12), 17359–17370.

Malin, M.C., Edgett, K.S., 2000. Evidence for recent groundwater seepage and surface runoff on Mars. Science 288 (5475), 2330–2335.

Malin, M.C., Edgett, K.S., 2001. Mars Global Surveyor Mars Orbiter Camera: Interplanetary cruise through primary mission. J. Geophys. Res. 106 (E10), 23429–23570.

Malin, M.C. et al., 2007. Initial observations by the MRO Mars Color Imager and Context Camera. Lunar Planet. Sci. XXXVIII, 2068.

Manning, R., 1891. On the flow of water in open channels and pipes. Trans. Inst. Civ. Eng. Ireland 20, 161–207.

Maxwell, T.A., Otto, E.P., Picard, M.D., Wilson, R.C., 1973. Meteorite impact: A suggestion for the origin of some stream channels on Mars. Geology 1 (1), 9–10.

McEwen, A.S., Preblich, B.S., Turtle, E.P., Artemieva, N.A., Golombek, M.P., Hurst, M., Kirk, R.L., Burr, D.M., Christensen, P.R., 2005. The rayed crater Zunil and interpretations of small impact craters on Mars. Icarus 176, 351–381.

McEwen, A.S. et al., 2007a. Mars Reconnaissance Orbiter's High Resolution Imaging Science Experiment (HiRISE). J. Geophys. Res. 112, E05S02.

McEwen, A.S. et al., 2007b. A closer look at water-related geologic activity on Mars. Science 317, 1706–1709.

Mellon, M.T., Jakosky, B.M., Postawko, S.E., 1997. The persistence of equatorial ground ice on Mars. J. Geophys. Res. 102 (E8), 19357–19369.

Mellon, M.T., Feldman, W.C., Prettyman, T.H., 2004. The presence and stability of ground ice in the southern hemisphere of Mars. Icarus 169, 324–340.

Melosh, H.J., 1989. Impact Cratering: A Geologic Process. Oxford University Press, New York, NY.

Melosh, H.J., Ivanov, B.A., 1999. Impact crater collapse. Annu. Rev. Earth Planet. Sci. 27, 385–415.

Morgan, G., Head, J.W., 2009. Sinton crater, Mars: Evidence for impact into a plateau icefield and melting to produce valley networks at the Hesperian–Amazonian boundary. Icarus 202, 39–59.

Mouginis-Mark, P.J., 1987. Water or ice in the martian regolith? Clues from rampart craters seen at very high resolution. Icarus 71, 268–286.

Mouginis-Mark, P.J., Garbeil, H., 2007. Crater geometry and ejecta thickness of the martian impact crater Tooting. Meteorit. Planet. Sci. 42 (9), 1615–1625.

Mouginis-Mark, P.J., Tornabene, L.L., Boyce, J.M., McEwen, A.S., 2007. Impact melt and water release at Tooting crater, Mars. In: 7th Int. Conf. on Mars, p. 3039.

Newsom, H.E., Graup, G., Sewards, T., Keil, K., 1986. Fluidization and hydrothermal alteration of the suevite deposit at the Ries crater, West Germany, and implications for Mars. J. Geophys. Res. 91 (B13), E239–E252.

Oberbeck, V.R., Morrison, R.H., 1973. On the formation of lunar herringbone pattern. Lunar Planet. Sci. IV (1), 107–123.

O'Connor, J.E., Webb, R.H., 1988. Hydraulic modeling for paleoflood analysis. In: Baker, V.R., Kochel, R.C., Patton, P.C. (Eds.), Flood Geomorphology. Wiley Interscience, New York, pp. 393–401.

Osinski, G.R., Lee, P., Parnell, J., Spray, J.G., Baron, M., 2005. A case study of impact-induced hydrothermal activity: The Haughton impact structure, Devon Island, Canadian High Arctic. Meteorit. Planet. Sci. 40 (12), 1859–1877.

Parker, T., 1996. Highlights from 1:500 K geologic mapping of central and southern Argyre Planitia. Lunar Planet. Sci. 27, 1003.

Poelchau, M.H., Kenkmann, T., 2008. Asymmetric signatures in simple craters as an indicator for an oblique impact vector. Meteorit. Planet. Sci. 43 (12), 2059–2072.

RIVIX, 2005. RiverTools Version 3.0.3 for Windows. Computer Software, Broomfield, CO.

Rodine, J.D., Johnson, A.M., 1976. The ability of debris, heavily freighted with coarse clastic materials, to flow on gentle slopes. Sedimentology 23, 213–234.

Senft, L.E., Stewart, S.T., 2008. Impact crater formation in icy layered terrains on Mars. Meteorit. Planet. Sci. 43 (12), 1993–2013.

Shoemaker, E.M., 1962. Interpretation of lunar craters. In: Kopal, Z. (Ed.), Physics and Astronomy of the Moon. Academic Press, New York, pp. 283–359.

Silberman, E., Carter, R., Einstein, H., Hinds, J., Powell, R., and ASCE Task Force on Friction Factors in Open Channels, 1963. Friction factors in open channels. J. Hydraul. Eng. 89 (HY2), 97–143.

Smith, P.H., 2009. Water at the Phoenix Landing Site. Ph.D. Thesis, The University of Arizona, Tucson, 39pp.

Smith, D.E. et al., 2001. Mars Orbiter Laser Altimeter: Experiment summary after the first year of global mapping of Mars. J. Geophys. Res. 106 (E10), 23689–23722.

Squyres, S.W., 1988. Urey prize lecture: Water on Mars. Icarus 79 (2), 229–288.

Stewart, S.T., Ahrens, T.J., 2005. Shock properties of H_2O ice. J. Geophys. Res. 110, E03005.

Tanaka, K.L., 1986. The stratigraphy of Mars. J. Geophys. Res. 91 (B13), E139–E158.

Tornabene, L.L., Moersch, J.E., McSween Jr., H.Y., McEwen, A.S., Piatek, J.L., Milam, K.A., Christensen, P.R., 2006. Identification of large (2–10 km) rayed craters on Mars in THEMIS thermal infrared images: Implications for possible martian meteorite source regions. J. Geophys. Res. 111, E10006.

Tornabene, L.L., McEwen, A.S., Grant, J.A., Mouginis-Mark, P.J., Squyres, S.W., Wray, J.J., and HiRISE Team, 2007a. Evidence for the role of volatiles on martian impact craters as revealed by HiRISE. Lunar Planet. Sci. XXXVIII, 2215.

Tornabene, L.L., McEwen, A.S., Osinski, G.R., Mouginis-Mark, P.J., Boyce, J.M., Williams, R.M.E., Wray, J.J., Grant, J.A., and HiRISE Team, 2007b. Impact melting and the role of subsurface volatiles: Implications for the formation of

valley networks and phyllosilicate-rich lithologies on early Mars. In: 7th Int. Conf. on Mars, p. 3288.
Tornabene, L.L., McEwen, A.S., and HiRISE Team, 2008. Recent channel systems emanating from Hale crater ejecta: Implications for the Noachian landscape evolution of Mars. Lunar Planet. Sci. XXXIX, 2180.
Tornabene, L.L., Moersch, J.E., McSween Jr., H.Y., Hamilton, V.E., Piatek, J.L., Christensen, P.R., 2008b. Surface and crater-exposed lithologic units of the Isidis Basin as mapped by coanalysis of THEMIS and TES derived data products. J. Geophys. Res. 113, E1001.
Williams, R., Malin, M., 2008. Sub-kilometer fans in Mojave Crater, Mars. Icarus 198, 365–383.
Williams, R.M.E., Zimbelman, J.R., Johnston, A.K., 2006. Aspects of alluvial fan shape indicative of formation process: A case study in southwestern California with application to Mojave Crater fans on Mars. Geophys. Res. Lett. 33, L10201.
Wilson, L., Ghatan, G.J., Head III, J.W., Mitchell, K.L., 2004. Mars outflow channels: A reappraisal of the estimation of water flow velocities from water depths, regional slopes, and channel floor properties. J. Geophys. Res. 109, E09003.